16th Australasian Fluid Mechanics Conference
Crown Plaza, Gold Coast, Australia
2-7 December 2007

High Speed Flow Control Using Microwave Energy Deposition

Doyle D. Knight[1], Yuri F. Kolesnichenko[2], Vadim Brovkin[2] and Dmitri Khmara[2]

[1]Department of Mechanical Engineering
Rutgers - The State University of New Jersey
New Brunswick, New Jersey USA

[2]Institute of High Temperatures
Russian Academy of Sciences
Moscow, RUSSIA

Abstract

In recent years a variety of beamed energy deposition techniques have been investigated for flow control in high speed flows. Among these, microwave energy deposition has been demonstrated experimentally to achieve significant drag reduction for blunt body flows. A gas dynamic model for microwave energy deposition in air is developed using 23 species and 238 reactions. The model is applied to the simulation of microwave energy deposition in supersonic flow past a cylinder.

Introduction

In recent years Electromagnetic Local Flow Control (ELFC) has received widespread research interest as an alternative to conventional methods of flow control in aerodynamics. ELFC includes a wide range of techniques including electron beam, laser, microwave, DC discharge and Dielectric Barrier Discharge (DBD), both without and with applied magnetic fields. Numerous papers have been presented at international conferences including the Weakly Ionized Gas Workshops (since 1997) in the United States, the Workshops on Magnetoplasma Aerodynamics for Aerospace Applications (since 1999) in Moscow, Russia, and the Workshops on Thermochemical Processes in Plasma Aerodynamics (since 2001) in St. Petersburg, Russia.

Three reviews have been published since the beginning of the series of conferences cited above. Zheltovodov [17] and Knight *et al.* [7] surveyed experimental and theoretical research on energy deposition for supersonic aerodynamic flow control up to the year 2002. The majority of the research was conducted in Russia including the former Soviet Union. The emphasis of the research was drag reduction, and both experiments and numerical simulations demonstrated conclusively that significant drag reduction can be achieved in supersonic flow concommitant with a net energy savings. Knight [8] surveyed experimental and theoretical research on Magneto Gas Dynamic (MGD) flow control in supersonic flows up to the year 2003 with a focus on the capability for reduction of drag and heat transfer in supersonic and hypersonic flows.

The objective of this paper is the application of a gas dynamic model for microwave energy deposition in air upstream of a cylinder at Mach 2 and the interaction of the microwave-generated plasma with the blunt body shock generated by the cylinder.

Microwave Energy Deposition for Flow Control

Microwave energy deposition has been shown to be an effective and energy-efficient method for drag reduction in supersonic flows [9]. Fig. 1 displays a sequence of Schlieren images for a microwave pulse upstream of a cylinder at Mach 2.1. The sequence displays the initial lensing of the bow shock as the thermal (plasma) region convects to and interacts with the bow shock. Fig. 2 shows the experimental centerline pressure *vs* time on a cylinder in Mach 2 due to the interaction of a microwave pulse with the cylinder. A significant momentary reduction in surface pressure (and hence drag) is evident.

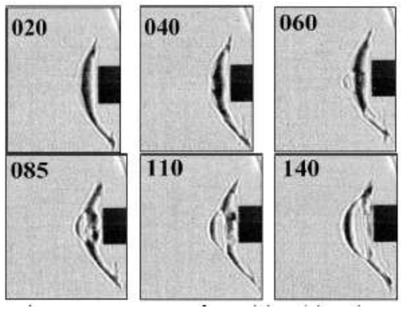

Figure 1: Microwave energy deposition (time in μs) ([11])

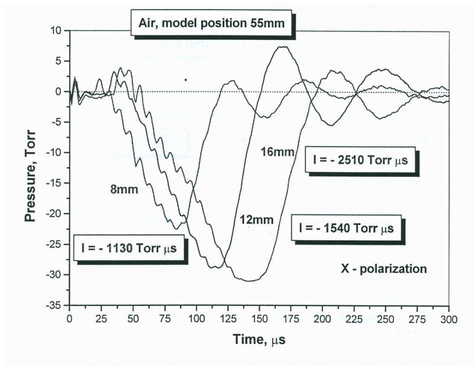

Figure 2: Surface pressure *vs* time ([9])

The plasma generated by microwave energy deposition is characterized by a warm ionized region surrounding a tangle of high temperature plasma filaments [2] as shown in Fig. 3. Both experiment (*e.g.*, Kolesnichenko *et al* [10]) and ideal gas numberical simulation (*e.g.*, Azarova *et al.* [1]) have demonstrated that the interaction of these filaments with the aerodynamic body (*i.e.*, the bow shock) are the mechanism for drag reduction. Control of the filament orientation by a laser precursor pulse or other technique is therefore essential. Indeed, the interaction of off-axis plasma filaments with blunt bodies has been demonstrated experimentally to cause an increase (rather than a decrease) in drag [11].

Several recent papers have examined the effect of laser energy deposition (laser spark) as a mechanism for both initiation and

Figure 3: Microwave filament ([2])

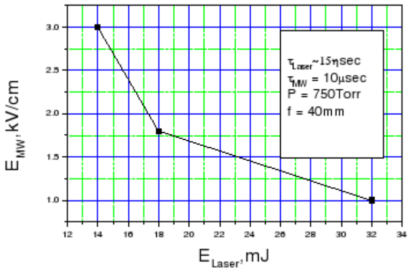

Figure 4: Microwave with laser ([3])

control of microwave energy deposition in air (*e.g.*, Mashek *et al.* [12], Brovkin *et al.* [2]). In particular, Brovkin *et al.* [3] have shown that a laser precursor can significantly reduce the microwave field needed for microwave discharge in air at atmospheric pressure. Fig. 4 shows the experimental results for the effect of a 15 ns Nd:YAG laser ($\lambda = 532$ nm) precursor spark on the microwave electric field required for microwave discharge in air at 750 Torr. A reduction of up to a factor of three in the microwave field is achieved. Additionally, the capability for remote generation of the microwave discharge was demonstrated [3].

Model for Simulation of Microwave Energy Deposition in Air

A fully three-dimensional, time-dependent gas dynamic model for microwave energy deposition in air has been developed incorporating detailed kinetics and thermochemistry. The following assumptions are employed:

1. Inviscid, non-heat conducting
2. Neglect relative diffusion of species in mass conservation
3. Neglect electron drift and diffusion
4. Neglect Lorentz force in momentum equation
5. Electric field is specified, and all properties are independent along $\vec{E}$
6. Coulomb force $\rho_c \vec{E}$ is omitted in momentum equation

The governing equations are listed below.

Mass

$$\frac{\partial \rho_i}{\partial t} + \frac{\partial \rho_i u_j}{\partial x_j} = \dot{\omega}_i \quad \text{for } i = 1, n \tag{1}$$

Momentum

$$\frac{\partial \rho u_i}{\partial t} + \frac{\partial \rho u_i u_j}{\partial x_j} = -\frac{\partial p}{\partial x_i} \quad \text{for } i = 1, 3 \tag{2}$$

Energy

$$\frac{\partial \rho \varepsilon}{\partial t} + \frac{\partial}{\partial x_j} (\rho \varepsilon + p) u_j = \dot{q} \tag{3}$$

Definitions

$$\varepsilon = H - \frac{p}{\rho} \tag{4}$$

$$H = h + \tfrac{1}{2} u_i u_i \tag{5}$$

$$h = \sum_{i \neq e} Y_i h_i \tag{6}$$

$$h_i = h^o_{f_i} + \int_{T_{\text{ref}}}^{T} c_{p_i} \, dT \tag{7}$$

$$p = \mathcal{R} T \sum_{i \neq e} \frac{\rho_i}{M_i} + N_e k T_e \tag{8}$$

$$\rho = \sum_{i \neq e} \rho_i \tag{9}$$

Reactions

$$\sum_{i=1}^{n} \nu'_{ik} \mathcal{M}_i \rightarrow \sum_{i=1}^{n} \nu''_{ik} \mathcal{M}_i \quad \text{for } k = 1, m \tag{10}$$

where $\mathcal{M}_i$ represents species i.

Rate of Production of Species

$$\dot{\omega}_i = M_i \sum_{k=1}^{m} \dot{c}_{i_k} \quad \text{for } i = 1, n \tag{11}$$

$$\dot{c}_{i_k} = \left(\nu''_{ik} - \nu'_{ik} \right) k_k \prod_{j=1}^{n} C_j^{\nu'_{jk}} \text{ for } i = 1, n;\ k = 1, m \tag{12}$$

$$C_j = \frac{\rho_j}{M_j} \quad \text{for } j = 1, n \tag{13}$$

Reaction Coefficients

The reaction coefficients k_k are obtained, after suitable conversion of units, from the reaction coefficients K_k defined by D. Khmara [6] according to

$$K_k = A X^n \exp\left(-\frac{B}{X} \right) \tag{14}$$

where X is the local gas temperature T (deg K), electron temperature T_e (deg K) or reduced field $\left.\frac{E}{\mathcal{N}}\right|_r$ (Townsend) depending upon the reaction; A, n and B are constants, and $\mathcal{N}$ is the total concentration (excluding N_e).

Rate of Gas Heating

The rate of gas heating per unit volume $\dot{q}$ is comprised of three contributions. First, the energy lost by electrons in elastic collision with heavy particles (*i.e.*, neutrals and ions) is [14]

$$\dot{q}_{\text{elastic}} = \tfrac{3}{2} k T_e \delta \nu_e N_e \tag{15}$$

where $\delta = 2m_e/M$ where m_e is the electron mass, M is a representative mass for the neutrals and ions, $\nu_e = \nu_c(1-\overline{\cos\theta})$ is the effective collision frequency (see below), and N_e is the electron concentration. The energy lost by electrons in elastic collisions with heavy particles is assumed to be completely transferred into heating of the gas (*i.e.*, the translational/rotational temperature of the gas).

Second, a fraction of the energy of the reactions is assumed to be completely transferred into heating of the gas

$$\dot{q}_{\text{reactions}} = \sum_{i=1}^{m} \alpha_i \Delta h_i \tag{16}$$

where α_i is the fraction of the rate of change of enthalpy per unit volume Δh_i for reaction i that goes into heating of the gas.

Third, the joule heating of the gas by the imposed microwave field is given by

$$\dot{q}_{\text{joule}} = \nu e \left.\frac{E}{\mathcal{N}}\right|_r \mathcal{N} V_{dr} N_e \tag{17}$$

where ν is the rotational relaxation factor, e is the electron charge, $\left.\frac{E}{\mathcal{N}}\right|_r$ is the reduced field, $\mathcal{N}$ is the total concentration of species (excluding electrons), and V_{dr} is the electron drift velocity.

Thus, the total energy added per unit volume per unit time is

$$\dot{q} = \tfrac{3}{2} k T_e \delta \nu_e N_e + \sum_{i=1}^{m} \alpha_i \Delta h_i + \nu e \left.\frac{E}{\mathcal{N}}\right|_r \mathcal{N} V_{dr} N_e \tag{18}$$

Reduced Field

$$\left.\frac{E}{\mathcal{N}}\right|_r = \frac{E(x_i,t)}{\mathcal{N}} \mu_1 \mu_2 \tag{19}$$

$$\mu_1 = \left[1 + \left(q \frac{N_e}{N_e^{crit}}\right)\right]^{-1/2} \tag{20}$$

$$\mu_2 = \frac{\nu_e}{\sqrt{\nu_e^2 + \omega^2}} \tag{21}$$

where q is the depolarization factor, N_e^{crit} is the critical electron concentration, ω is the microwave angular frequency (rad/sec), and ν_e is the effective frequency of electron collisions with reagents given by

$$\nu_e = \mathcal{N} K_{\nu_e} \tag{22}$$

where

$$K_{\nu_e} = \exp\left[\sum_{i=0}^{9} a_i \left(\log_e \left.\frac{E}{\mathcal{N}}\right|_r\right)^i\right] \tag{23}$$

where ν_e is in s^{-1}, $\left.\frac{E}{\mathcal{N}}\right|_r$ is in Townsend, $\mathcal{N}$ is the concentration in cm^{-3} (neglecting electrons) and a_i are specified constants. Equation (19) is an implicit equation for $\left.\frac{E}{\mathcal{N}}\right|_r$ and is solved by Newton's method. The expression for K_{ν_e} is shown in Fig. 5.

Electron Temperature

$$T_e = \exp\left[\sum_{i=0}^{9} b_i \left(\log_e \left.\frac{E}{\mathcal{N}}\right|_r\right)^i\right] \tag{24}$$

where T_e is in eV, $\left.\frac{E}{\mathcal{N}}\right|_r$ is in Townsend, and b_i are specified constants. The expression is shown in Fig. 6. Electrons are assumed to thermalize instantaneously ($T_e = T$) when $E = 0$.

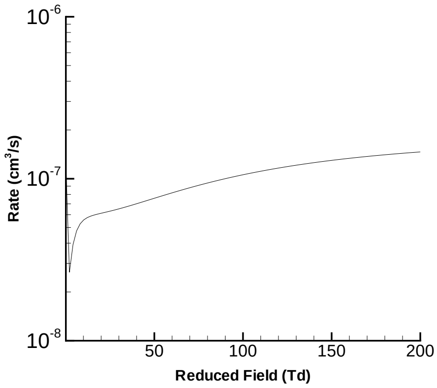

Figure 5: K_{ν_e} *vs* $\left.\frac{E}{\mathcal{N}}\right|_r$

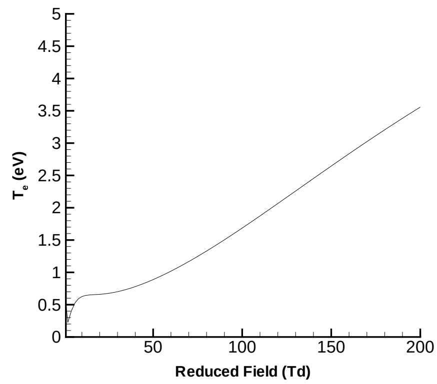

Figure 6: T_e *vs* $\left.\frac{E}{\mathcal{N}}\right|_r$

Drift Velocity

$$V_{dr} = \exp\left[\sum_{i=0}^{9} c_i \left(\log_e \left.\frac{E}{\mathcal{N}}\right|_r\right)^i\right] \tag{25}$$

where V_{dr} is in cm/s, $\left.\frac{E}{\mathcal{N}}\right|_r$ is in Townsend, and c_i are specified constants. The expression is shown in Fig. 7.

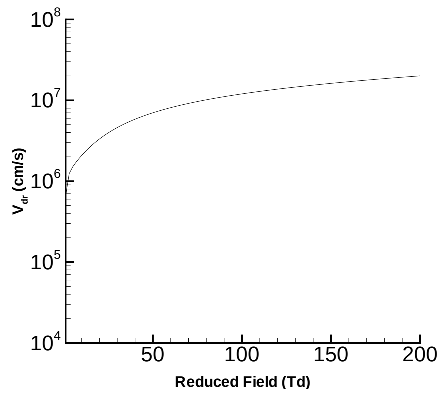

Figure 7: V_{dr} *vs* $\left.\frac{E}{\mathcal{N}}\right|_r$

Rotational Relaxation Factor

$$\nu = d_o \left(\frac{E}{N}\bigg|_r \right)^{d_1} \exp\left(-d_2 / \frac{E}{N}\bigg|_r \right) \qquad (26)$$

where ν is dimensionless, $\frac{E}{\mathcal{N}}\Big|_r$ is in Townsend, and d_i are specified constants. The expression is shown in Fig. 8.

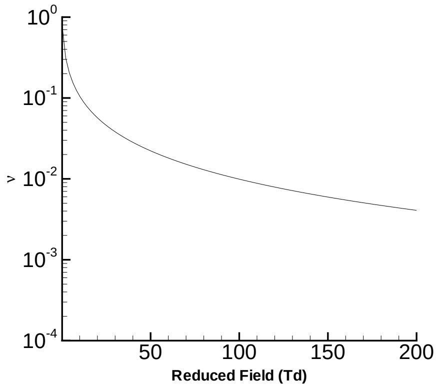

Figure 8: ν *vs* $\frac{E}{\mathcal{N}}\Big|_r$

Electric Field

$$E = \begin{cases} E_o \left[1 - (r/r_o)^2 \right] f(t) & 0 < r \le r_o \\ 0 & r_o < r \end{cases} \qquad (27)$$

where r is the spherical radius and $f(t)$ is the dimensionless temporal behavior defined by

$$f(t) = \begin{cases} 1 & 0 < t < \tau_o \\ 1 - (t - \tau_o)/(\tau_1 - \tau_o) & \tau_o < t < \tau_1 \\ 0 & t > \tau_1 \end{cases} \qquad (28)$$

Note that the electric field decreases linearly in time from $t = \tau_o$ to $t = \tau_1$.

The drift velocities of individual species are neglected due to the high frequency of the electric field and because the electric field vector is assumed perpendicular to the mass flow velocity. Charge separation is neglected (and hence the Coulomb force $\rho_c E$ is omitted) because diffusion has been neglected and the electric field vector is assumed perpendicular to the mass flow velocity vector.

The kinetic model [5] incorporates 23 species (e^-, N_2, O_2, NO, N, O, $N_2(A^3\Sigma_u+)$, $N_2(B^3\Pi_g)$, $N_2(C^3\Pi_u)$, $N_2(a'^1\Sigma_u^-)$, $O(^1D)$, $O(^1S)$, $N(^2D)$, $N(^2P)$, N_2^+, O_2^+, NO^+, N_4^+, N^+, O^+, O_2^-, O^- and O_3^-) and 238 reactions. The kinetic model was validated by comparison with experimental data for microwave discharge in quiescent air at 70 Torr and an initial gas temperature $T_g = 200$ deg K. The model accurately predicted the final gas temperature within 10 deg K.

The governing equations are solved using a cell-centered structured multiblock code developed by the first author. The inviscid fluxes are discretized using Roe's method extended for multiple species and including a compatability condition for determination of the static pressure [13]. Temporal integration is performed using a second-order accurate semi-implicit Runge-Kutta method [18]. The code is parallelized using Message Passing Interface (MPI) [4] and runs on an AMD-64-based cluster under Debian Linux.

Simulation of Interaction of Microwave Discharge with Flow Past a Cylinder at Mach 2

A simulation of the interaction of a microwave energy discharge with the flow past a cylinder at $M_\infty = 2$ was performed. Fig. 9 shows the flow configuration and the location of the microwave pulse. The microwave energy deposition generates a blast wave that propagates spherically outwards while the heated plasma convects downstream and interacts with the blunt body shock ahead of the cylinder. The flow conditions are shown in Table 1 including the initial concentrations of N_2, O_2, O_2^+ and e which were taken to be uniform in the freestream prior to the pulse. The initial concentration of all other species was set to zero. The cylinder diameter is $D = 3$ cm. The freestream conditions correspond to recent experiments of Lashkov *et al* [11]). The depolarization factor q was set to zero to simulate the formation of the microwave filament at the core of the discharge. The discharge was assumed to be spherically symmetric and centered at $x_o = -3$ cm upstream of the cylinder.

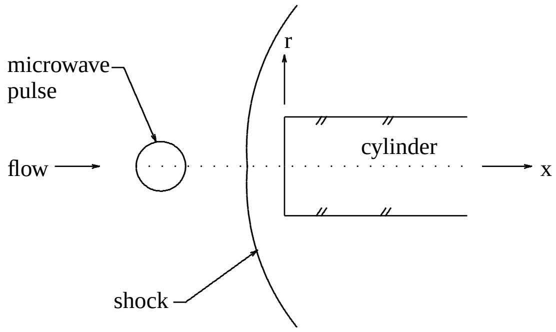

Figure 9: Flow configuration

Parameter	*Value*
M_∞	2.0
p_∞ (Torr)	40.57
T_∞ (deg K)	200
ρ_∞ (kg/m^3)	$9.25 \cdot 10^{-2}$
D (cm)	3
N_{N_2} (cm^{-3})	$1.526 \cdot 10^{18}$
N_{O_2} (cm^{-3})	$0.406 \cdot 10^{18}$
$N_{O_2^+}$ (cm^{-3})	$3.0 \cdot 10^4$
N_e (cm^{-3})	$3.0 \cdot 10^4$
E_o (kV/cm)	2.75
r_o (cm)	1.5
x_o (cm)	-3.0
$\omega/2\pi$ (GHz)	10
τ_o (μs)	1.00
τ_1 (μs)	1.01
q	0

Table 1: Flow Conditions for MW Discharge in Supersonic Flow Past a Cylinder

The temporal evolution of the pressure p, gas temperature T and electron tempreature T_e at the center of the discharge is shown in Fig. 10 together with the imposed electric field. The gas temperature and pressure begin to rise rapidly at $t = 1$ μs. The pressure reaches a peak value of 575.5 Torr at $t = 1.23$ μs, and the gas temperature reaches its maximum value of 2507 deg K at $t = 1.33$ μs. The temporal evolution of the gas heating contributions $\dot{q}_{\text{elastic}}, \dot{q}_{\text{reactions}}$ and $\dot{q}_{\text{joule}}$ at the center of the microwave discharge are shown in Fig. 11. The most significant contribution during the period of microwave discharge ($0 \le t \le \tau_1$) is $\dot{q}_{\text{reactions}}$ which reaches a maximum value of 1.84 MW/cm^3.

The corresponding maximum values for $\dot{q}_{\text{elastic}}$ and $\dot{q}_{\text{joule}}$ are 0.031 MW/cm^3 and 0.31 MW/cm^3, respectively.

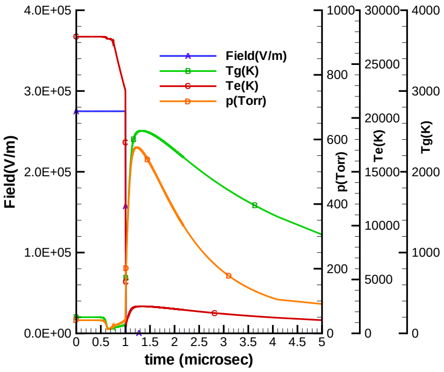

Figure 10: p, T, T_e and E *vs* t

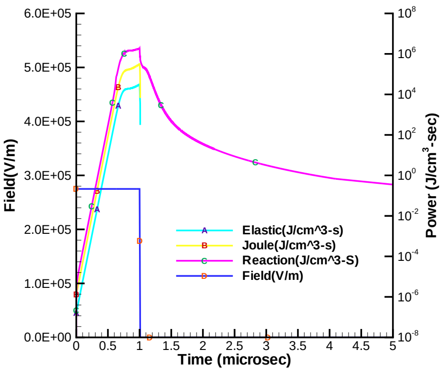

Figure 11: $\dot{q}_{\text{elastic}}, \dot{q}_{\text{reactions}}, \dot{q}_{\text{joule}}$ and E *vs* t

Figs. 12 and 13 display pressure contours[1] at $t = 1.55$ μs and 12.1 μs after the initiation of the microwave pulse[2]. The blunt body shock generated by the cylinder is evident. The plasma is indicated by the spherical high pressure region upstream of the blunt body shock. The blast wave propagates spherically outwards with a concommitant inward expansion wave resulting in a rapid reduction of the pressure inside the plasma. The pressure on the cylinder face at the centerline (relative to the undisturbed pressure p_o at the same location) *vs* time is displayed in Fig. 14. The initial pressure rise at $t = 35$ μs is due to the interaction of the blast wave with the cylinder face. The subsequent expansion is associated with the formation of a torodial vortex (see below). The maximum decrease in pressure is 50 Torr which is comparable to values achieved in experiment (Fig. 2) under similar (but not identical) conditions to the simulation.

Figs. 15 to 19 display static temperature contours at $t = 1.55$ μs, 12.1 μs, 49.1 μs and 112.9 μs. The interaction of the hot plasma with the blunt body shock (Figs. 16 to 17) causes a lensing forward of the blunt body shock and the momentary formation of a toroidal vortex as indicated in the instantaneous streamlines (Fig. 18). The formation of the vortex coincides with a reduction in the surface pressure on the cylinder (Fig. 14) and is qualitatively similar to previous computations using the Euler equations [1].

[1]Contour plots display only the upper half of the domain (*i.e.*, $r \geq 0$).

[2]The flowfield was initially converged to steady state. The microwave pulse starts at $t = 0$ and ends at $t = 1.01$ μs.

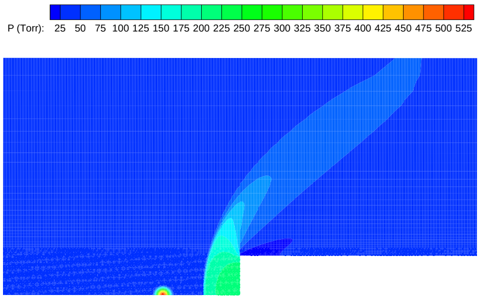

Figure 12: p at $t = 1.55$ μs

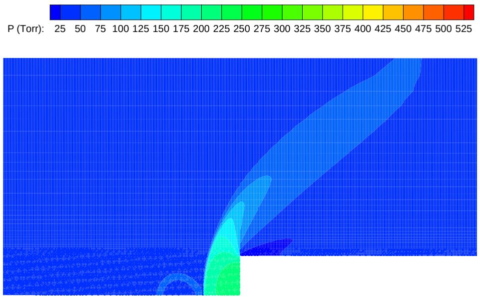

Figure 13: p at $t = 12.1$ μs

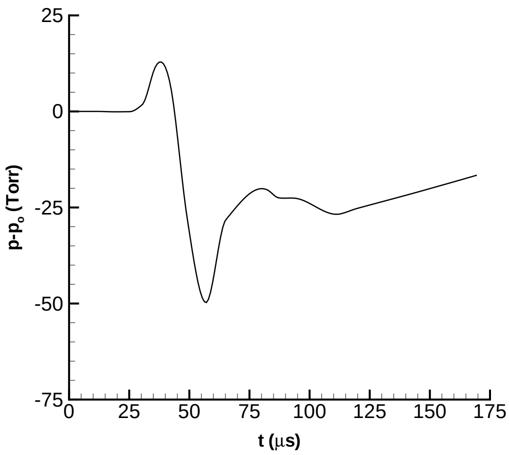

Figure 14: p *vs* t on centerline

Figs. 20 to 23 display contours of atomic oxygen O at $t = 1.55$ μs, 12.1 μs, 49.1 μs and 112.9 μs. The microwave pulse causes an immediate dissociation of O_2. At $t = 1.55$ μs, the peak concentration of O is $6.12 \cdot 10^{17}$ cm^{-3} which is 1.51 times the initial concentration of O_2, thereby indicating significant dissociation of molecular oxygen within the plasma formed by the microwave beam. This level remains relatively high with a peak O concentration of $3.91 \cdot 10^{16}$ cm^{-3} at $t = 112.9$ μs.

Figs. 24 to 28 display contours of NO at $t = 1.55$ μs, 12.1 μs, 49.1 μs and 112.9 μs. At $t = 1.55$ μs, the peak concentration

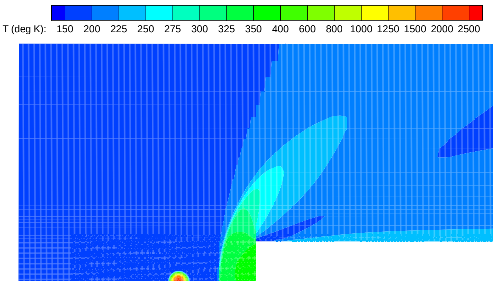

Figure 15: T at $t = 1.55$ μs

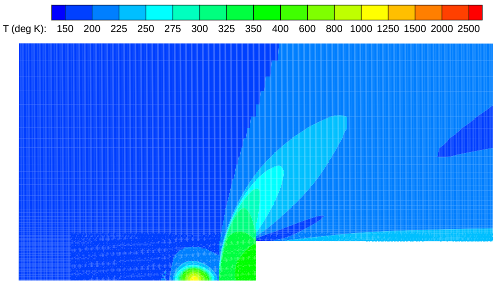

Figure 16: T at $t = 12.1$ μs

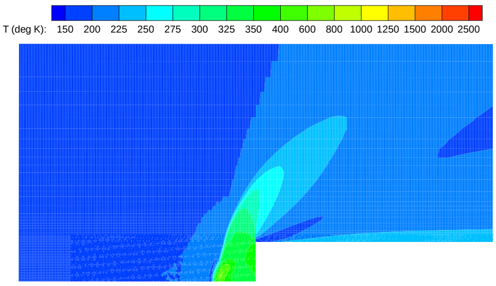

Figure 17: T at $t = 49.1$ μs

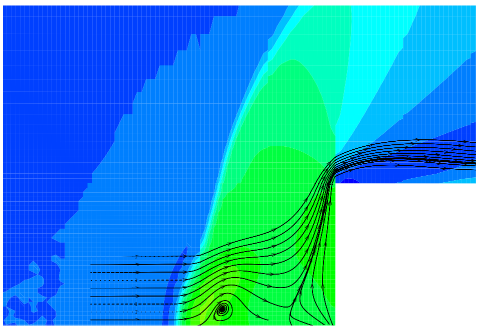

Figure 18: T at $t = 49.1$ μs with streamlines

of NO is $2.3 \cdot 10^{16}$ cm^{-3}; however, by $t = 112.9$ μs, the peak concentration has decreased to $5.4 \cdot 10^{14}$ cm^{-3}.

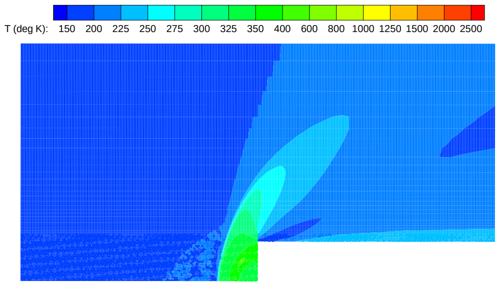

Figure 19: T at $t = 112.9$ μs

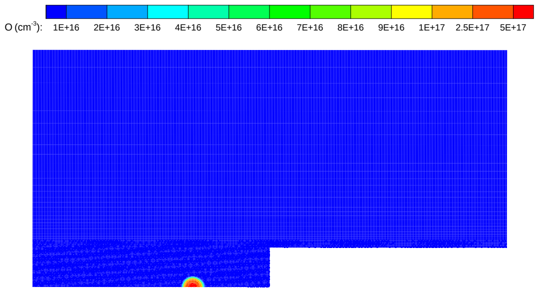

Figure 20: O at $t = 1.55$ μs

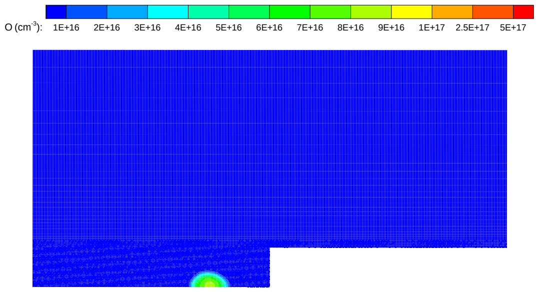

Figure 21: O at $t = 12.1$ μs

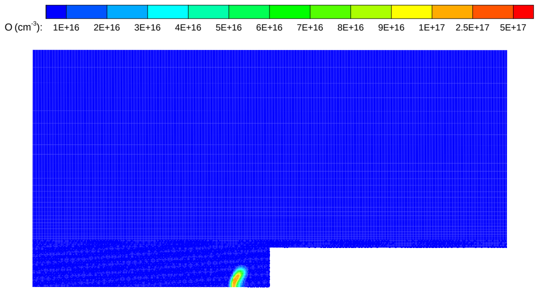

Figure 22: O at $t = 49.1$ μs

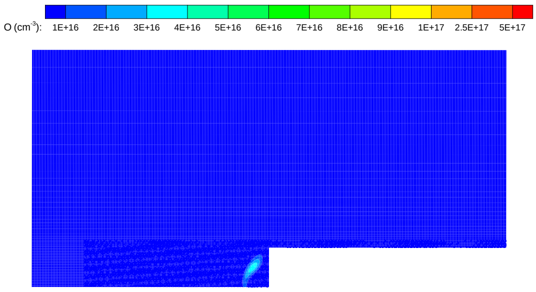

Figure 23: O at $t = 112.9$ μs

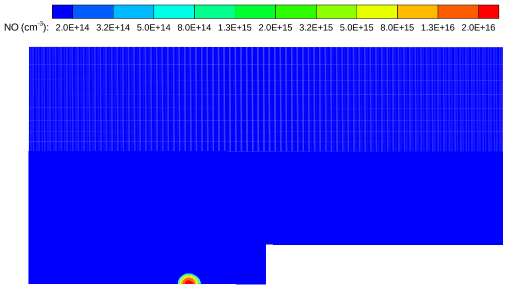

Figure 24: NO at $t = 1.55$ μs

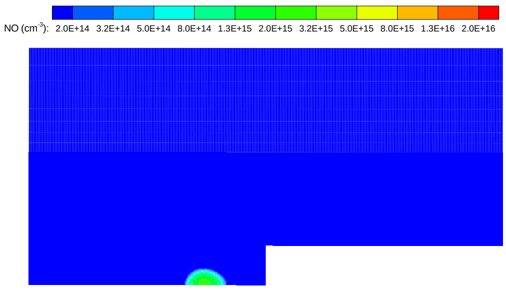

Figure 25: NO at $t = 12.1$ μs

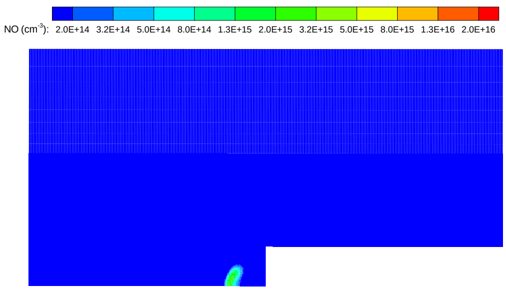

Figure 26: NO at $t = 49.1$ μs

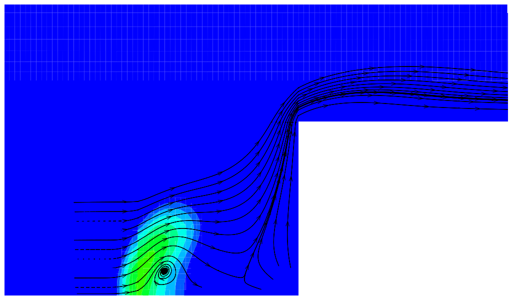

Figure 27: NO at $t = 49.1$ μs with streamlines

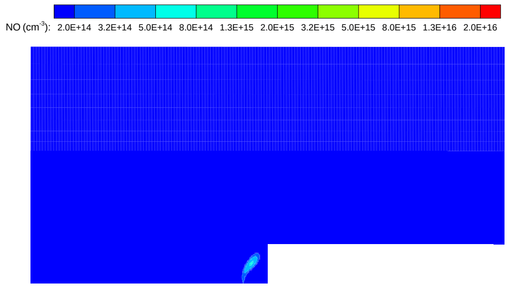

Figure 28: NO at $t = 112.9$ μs

Conclusions

A gas dynamic model for microwave energy deposition in air is developed. The model includes detailed kinetics and thermochemistry using 23 species and 238 reactions. The model is implemented in a fully three-dimensional flow code using Roe's method (extended for multiple species) for the inviscid fluxes and a semi-emplicit Runge-Kutta algorithm for time integration. The code is parallelized using MPI. The model is applied to the simulation of microwave energy deposition in Mach 2 flow upstream of a blunt cylinder. The interaction of the heated plasma (generated by the microwave pulse) with the blunt body shock results in the momentary formation of a toroidal vortex and reduction in the stagnation pressure on the cylinder centerline in agreement with experiment. Substantial dissociation of O_2 occurs due to the microwave discharge and high levels of O remain throughout the interaction. A significant concentration of NO forms initially but rapidly decays.

Acknowledgments

The research was supported by AFOSR Grant FA9550-07-1-0228 (monitored by Dr. John Schmisseur), the United States Air Force European Office of Scientific Research (monitored by Dr. Surya Surampudi), and the Russian Academy of Sciences.

References

[1] Azarova, O., Grudnitsky, V. and Kolesnichenko, Y., "Some Gas Dynamic Aspects of Flow Control by MW Energy Deposition", Proc. of Sixth Workshop on Magnetoplasma Aerodynamics for Aerospace Applications, Moscow, Russia, 2005, pp. 152–163.

[2] Brovkin, V., Afanas'ev, S., Khmara, D. and Koles-

nichenko, Y., "Microwave Discharge Control by Magnetic Field", AIAA Paper No. 2004-0357, January 2004.

[3] Brovkin, V., Afanas'ev, S., Khmara, D. and Kolesnichenko, Y., "Experimental Investigation of Combined Laser-DC-MW Discharges", AIAA Paper No. 2006-1459, January 2006.

[4] Grop, W. *et al.*, *MPICH2 User's Guide*, Version 1.0.5, Mathematics and Computer Science Division, Argonne National Laboratory, December 2006.

[5] Khmara, D., Kolesnichenko, Y. and Knight, D., "Modeling of Microwave Filament Origination", AIAA Paper No. 2006-0794, January 2006.

[6] Khmara, D., Kolesnichenko, Y. and Knight, D., "A Kinetic Model of Microwave Energy Deposition in Air", Fifth Workshop on Thermochemical Processes in Plasmadynamics, Leninetz Holding Co., St. Petersburg, Russia, June 2006.

[7] Knight, D., Kuchinskiy, V., Kuranov, A., and Sheikin, E., "Survey of Aerodynamic Flow Control at High Speed Using Energy Addition", AIAA Paper No. 2003-0525, January 2003.

[8] Knight, D., "Survey of Magneto-Gasdynamic Local Flow Control at High Speeds", AIAA Paper No. 2004-1191, January 2004.

[9] Kolesnichenko, Y., Brovkin, V., Azarova, O., Brudnitsky, V., Lashkov, V. and Mashek, I., "Microwave Energy Release Regimes for Drag Reduction in Supersonic Flows", AIAA Paper No. 2002-0353, January 2002.

[10] Kolesnichenko, Y., Azarova, O., Brovkin, V., Khmara, D., Lashkov, V., Mashek, I. and Ryvkin, M., "Basics in Beamed MW Energy Deposition for Flow/Flight Control", AIAA Paper No. 2004-669, January 2004.

[11] Lashkov, V., Mashek, I., Anisimov, Y., Ivanov, V., Kolesnichenko, Y., Ryvkin, M., and Gorynya, A., "Gas Dynamic Effect of Microwave Energy Discharge on Supersonic Cone Shaped Bodies", AIAA Paper No. 2004-0671, January 2004.

[12] Mashek, I., Anisimov, Y., Lashkov, V., Kolesnichenko, Y., Brovkin, V. and Rivkin, M., "Microwave Discharge Initiated by Laser Spark in Air", AIAA Paper No. 2004-0358, January 2004.

[13] Molvik, G. and Merkle, C., "A Set of Strongly Coupled, Upwind Algorithms for Computing Flows in Chemical Nonequilibrium", AIAA Paper No. 89-0199, 1989.

[14] Raizer, Y., *Gas Discharge Physics*, Springer, New York, 1991.

[15] Sedov, L., *Similarity and Dimensional Analysis in Mechanics*, M. Holt (Ed.), Academic Press, New York, 1959 (translated from Russian).

[16] Taylor, G., "The Formation of a Blast Wave by a Very Intense Explosion", *Proc. Royal Society of London*, A201, 1950, pp. 159–174.

[17] Zheltovodov, A., "Development of the Studies on Energy Deposition for Application to the Problems of Supersonic Aerodynamics", Preprint No. 10-2002, Khristianovich Institute of Theoretical and Applied Mechanics, Novosibirsk, Russia, 2002.

[18] Zhong, X., "Additive Semi-Implicit Runge-Kutta Methods for Computing High-Speed Nonequilibrium Reactive Flows", *Journal of Computational Physics*, Vol. 128, 1996, pp. 19–31.

Variable	*Quantity*
$\dot{c}_{i_k}$	rate of production of species i from reaction k
c_{p_i}	specific heat at constant pressure for species i
C_i	molar concentration of species i
ε	total energy per unit mass of mixture
E	electric field (E_o maximum electric field)
$\left.\frac{E}{\mathcal{N}}\right\|_r$	reduced field
$h^o_{f_i}$	heat of formation of species i at temperature T_{ref}
h_i	static enthalpy of species i per unit mass of species i
h	static enthalpy per unit mass of mixture
H	total enthalpy per unit mass of mixture
k	Boltzman constant ($1.38 \cdot 10^{-23}$ J/K)
k_k	reaction coefficient for reaction k
M_i	molecular weight of species i (kg/kg·mole)
$\mathcal{M}_i$	species i (*e.g.*, $\mathcal{M}_1 = e$)
m	number of reactions
m_e	mass of electron
M	representative mass for ions and neutrals
N_e	electron concentration
N_e^{crit}	critical electron concentration
N_i	concentration of species i
$\mathcal{N}$	total concentration of species excluding electrons
n	number of species including electrons
p	static pressure
$\dot{q}$	rate of heating of gas per unit volume
r_o	radius of microwave discharge
$\mathcal{R}$	universal gas constant (8314 J/kg·mole K)
T	static (translational) temperature of mixture
T_e	electron temperature
T_{ref}	reference temperature
u_i	mass-averaged velocity component in i-direction
V_{dr}	drift velocity
x_i	Cartesian coordinate
Y_i	mass fraction of species i ($Y_i = \rho_i/\rho$)
α_i	fraction of the rate of change in enthalpy Δh_i converted into heating of gas
δ	$2m_e/M$
Δh_i	rate of change in enthalpy due to reaction i
λ	wavelength of microwave
ρ_c	charge density
ρ_i	density of species i
ρ	density of mixture
$\dot{\omega}_i$	net rate of production of species i
ω	microwave angular frequency
ν	rotational relaxation factor (dimensionless)
ν_e	effective frequency of electron collisions
ν'_{ik}, ν''_{ik}	reaction coefficients
τ_o, τ_1	time scales in microwave discharge
$\sum_{i \neq e}$	sum over all species except electrons

Table 2: Nomenclature